Available online at www.sciencedirect.com
ScienceDirect
Computerized Medical Imaging and Graphics 31 (2007) 643–655
Computerized Medical Imaging and Graphics
www.elsevier.com/locate/compmedimag

Hip cartilage thickness measurement accuracy improvement

Yuanzhi Cheng [a,b,c,*], Shuguo Wang [b], Takaharu Yamazaki [c,d], Jie Zhao [b], Yoshikazu Nakajima [e], Shinichi Tamura [c,d]

[a] School of Computer Science and Technology, Harbin Institute of Technology in Weihai, China
[b] Mechareonic Engineering Department Robitics Institute, Harbin Institute of Technology, China
[c] Division of Image Analysis, Osaka University Graduate School of Medicine, Japan
[d] Center for Advanced Medical Engineering and Informatics, Osaka University, Japan
[e] Department of Bioengineering, School of Engineering, University of Tokyo, Japan

Received 6 December 2005; received in revised form 27 July 2007; accepted 2 August 2007

Abstract

Accurate measurement of the distance separating two adjacent sheet structures, such as femoral cartilage and acetabular cartilage in the hip joint is important in evaluation of osteoarthritis. A new method, insensitive to the influence of adjacent sheet structures, was developed to improve the accuracy of hip cartilage thickness measurement. A theoretical simulation for investigating the influence of adjacent sheet structures on the accuracy of cartilage thickness measurement in MR images was performed. The thickness is defined as the distance between zero-crossings of the second directional derivatives along the sheet surface normal direction. The simulation measurement showed considerable underestimation in thickness measurement occurred due to the influence of the adjacent sheet. A new method based on a model of the MR imaging process to eliminate the influence of adjacent sheet structure was developed and tested using phantoms and two cadaveric human hip joint MR scans. The new method reduced the influence of the adjacent sheet structure was more accurate than the conventional method for measuring hip cartilage thickness.

Keywords: Cartilage thickness; Point spread function; Measurement accuracy; Theoretical simulation; Line filter responses; Second directional derivative; Zero-crossings

1. Introduction

Accurate thickness measurement of sheet-like (or plate-like) thin anatomical structures, such as articular cartilage, has become increasingly important in clinical applications. Osteoarthritis or posttraumatic articular injuries can result in changes to the morphology of articular cartilage. Measuring and monitoring changes of articular cartilage thickness can play a critical role in the management of patients with disease or injury to those tissues.

The majority of studies for measuring the articular cartilage thickness have focused on the knee joint [1–5], where the cartilage surfaces do not fit tightly. Only a limited number of studies have addressed cartilage abnormalities in the hip joint [6,7]. In the hip, both the femoral head and the acetabulum are covered with cartilage. The ball and socket constitution of the hip joint, with strong capsule and ligaments, does not permit discrimination of the articular cartilage of the femoral head from the acetabulum. To allow separation of acetabular and femoral cartilages in MR images, the original continuous leg traction technique was used during MR imaging [8]. However, in many cases, the joint space between the femoral cartilage and acetabular cartilage is narrow despite traction. In a related study, in case two tubular structures are close to each other, Krissian et al., analyzed the cause of its influence on centerline detection of tubular structures [9]. Therefore, for the two articular cartilages of the hip joint, it is imperative to investigate whether one can impose a limitation on the accuracy of thickness measurement, but no studies as of yet have assessed this limitation.

In this paper, we develop a mathematical model for two adjacent sheet structures based on the (one-dimensional) 1D signal intensity profile along the normal direction of two sheet structures separated by a small distance, and then perform numerical simulation of MR imaging and postprocessing for thickness

* Corresponding author at: School of Computer Science and Technology, Harbin Institute of Technology in Weihai, No. 2 Wenhuaxi Road, Weihai 264209, China. Tel.: +86 631 5687578; fax: +86 631 5687506.
E-mail address: yz_cheng@image.med.osaka-u.ac.jp (Y. Cheng).

0895-6111/$ – see front matter © 2007 Elsevier Ltd. All rights reserved.
doi:10.1016/j.compmedimag.2007.08.001

measurement. The thickness is defined as the distance between the two sides of the edges, which are the zero-crossings points of the second directional derivatives along the normal direction. We compare the measured thickness of a single sheet structure with that of the sheet structure influenced by the adjacent sheet structure and confirm that considerable underestimation error in thickness measurement occurred due to the influence of the adjacent sheet structure. To improve measurement accuracy, we propose a new measurement technique based on matching a modeled intensity profile with an actual intensity profile observed in the MR data set. Using the phantoms and two cadaveric human hip joints, we present results showing that the influence of the adjacent sheet structure is eliminated, and the improved technique is more accurate than the conventional zero-crossings method in measuring the thickness of two adjacent sheet structures.

2. Methods and materials

2.1. Theoretical simulation studies

2.1.1. Mathematical model definition

Let Sheet_1 and Sheet_2 represent the two adjacent sheet structures, which model the two cartilages in the hip joint. Fig. 1a shows a 2D representation of two adjacent sheet structures on the x–y plane. In this study, our investigations will focus on assessing the influence of Sheet_1 on thickness measurement of Sheet_2 in two dimensions (on the x–y plane). In Fig. 1a, the in-plane rotation angle θ is defined as the angle formed by the x-axis and the sheet normal direction $\vec{r}_\theta$, where $\vec{r}_\theta = (\cos\theta, \sin\theta)$. The 1D profile of the ideal density distributions of two adjacent sheets, along the x-axis (normal direction of sheet surface), can be expressed as

$$P_n(x;\tau_1,\tau_0,\tau_2) = \begin{cases} D_b, & x < -\tau_1 - \tau_0/2 \\ D_t, & -\tau_1 - \tau_0/2 \le x \le -\tau_0/2 \\ D_0, & -\tau_0/2 < x < \tau_0/2 \\ D_t, & \tau_0/2 \le x \le \tau_0/2 + \tau_2 \\ D_b, & x > \tau_0/2 + \tau_2 \end{cases}, \quad (1)$$

and two adjacent sheets perpendicular to the x-axis, can be modeled as:

$$S_0(X;\tau_1,\tau_0,\tau_2) = P_n(x;\tau_1,\tau_0,\tau_2). \quad (2)$$

where $X=(x,y)^T$, τ_0, τ_1 and τ_2 represent the distance between two adjacent sheets, Sheet_1 thickness and Sheet_2 thickness, respectively. D_b, D_t and D_0 denote the density distributions of the background of both sides, two adjacent sheets and the space between them, respectively (Fig. 1b). Two adjacent sheets with direction $\vec{r}_\theta$ can be written as:

$$S(X;\tau_1,\tau_0,\tau_2,\vec{r}_\theta) = S_0(X';\tau_1,\tau_0,\tau_2), \quad (3)$$

and

$$X' = R_\theta X. \quad (4)$$

where R_θ denotes a 2×2 matrix representing rotation θ around the z-axis.

2.1.2. MR imaging model generation

The spatial resolution of MR system can be characterized by 2D point spread function (PSF). The MR imaging of two adjacent sheets are given by

$$I_{\text{model}}(X;\tau_1,\tau_0,\tau_2,) = S(X;\tau_1,\tau_0,\tau_2,\vec{r}_\theta) \otimes \text{PSF}(X;\Delta_x,\Delta_y), \quad (5)$$

where $I_{\text{model}}(X;\tau_1,\tau_0,\tau_2)$ is the MR imaging of two adjacent sheets, $\otimes$ denotes the convolution operation. Δ_x and Δ_y represent sampling intervals along the x- and y-axis, respectively. The 2D point spread function PSF $(X;\Delta_x,\Delta_y)$ can be represented by

$$\text{PSF}(x;\Delta_x,\Delta_y) = \text{PSF}(x;\Delta_x)\text{PSF}(y;\Delta_y), \quad (6)$$

The 1D point spread function PSF $(x;\Delta_x)$ along the x-axis, is defined as follows [10]:

$$\text{PSF}(x;\Delta_x) = \frac{1}{N_x}\frac{\sin\left(\pi\frac{x}{\Delta_x}\right)}{\sin\left(\pi\frac{x}{N_x\Delta_x}\right)}, \quad (7)$$

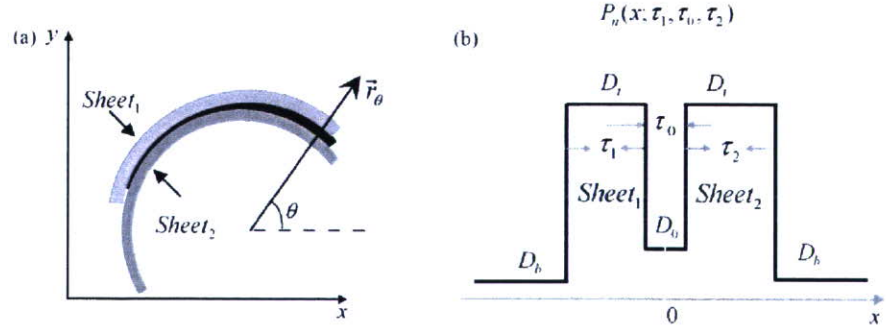

Fig. 1. The ideal model of two adjacent sheet structures. (a) 2D representation of two adjacent sheet structures. Sheet_1 and Sheet_2 represent the acetabular and femoral cartilages, respectively. The normal direction of the sheet surface is expressed as $\vec{r}_\theta = (\cos\theta, \sin\theta)$, where θ is the in-plane rotation angle. (b) 1D profile of ideal intensity distributions along the normal orientation of sheet surface for two adjacent sheets. τ_1, τ_2 and τ_0 are Sheet_1 thickness, Sheet_2 thickness and distance between them, respectively. D_b, D_t and D_0 denote the ideal intensity of the background of both sides, that of the two adjacent sheets and that of the region between them, respectively.

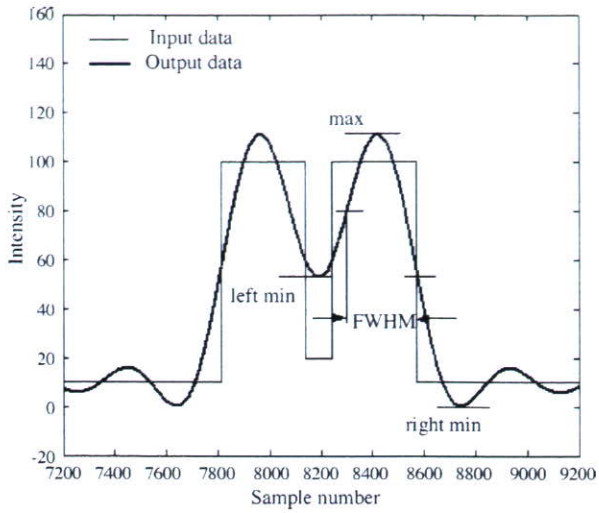

Fig. 2. 1D profile of ideal density values (input data) and MR intensity values (output data) along the normal direction, with the spatial resolution of $\Delta_x = \Delta_y = 0.625$. Note that FWHM method underestimated the thickness of Sheet$_2$.

where N_x is the number of samples in the frequency domain. Eq. (7) is well-approximated by

$$\mathrm{PSF}(x; \Delta_x) = \frac{1}{N_x} \frac{\sin\left(\pi \frac{x}{\Delta_x}\right)}{\pi \frac{x}{\Delta_x}}. \tag{8}$$

2.1.3. Distribution of MR intensity at the normal line

The effects of MR imaging and limited in-plane resolution can be elucidated by analyzing 1D profile of MR intensity values, $I_{\mathrm{model}}(X; \tau_1, \tau_0, \tau_2)$, along the normal direction θ. We assume that a parameter s denotes the position on the straight line, given by

$$X = s \cdot \vec{r}_\theta. \tag{9}$$

Thus, by substituting Eq. (9) for X in $I_{\mathrm{model}}(X; \tau_1, \tau_0, \tau_2)$

$$I_{\mathrm{model}}(s; \tau_1, \tau_0, \tau_2) = I_{\mathrm{model}}(s \cdot \vec{r}_\theta; \tau_1, \tau_0, \tau_2) \tag{10}$$

is derived. Fig. 2 shows 1D profiles of the density values (input data) $P_n(x; \tau_1, \tau_0, \tau_2)$ and MR intensity values (output data) $I_{\mathrm{model}}(s; \tau_1, \tau_0, \tau_2)$ at the normal direction $\theta = 0°$.

To explain the influence of Sheet$_1$ on the accuracy in thickness measurement of Sheet$_2$, we exhibit a profile of full-width-half-maximum (FWHM) [11–13] filter responses besides a profile of the second derivative responses described in the following Section 2.1.4. FWHM calculates a "half height point" on the left and right sides of the initial determined mid-point of profile. On each side, the minimum and maximum intensity values are calculated, and the "half height point" is located where the profile crosses the mid-point in intensity between the minimum and maximum. FWHM estimation of the profile width is defined as the distance between these half height points (Fig. 2).

2.1.4. Procedure for thickness measurement by zero-crossings method

To illustrate the potential measurement errors when applying the zero-crossings method for two adjacent sheets, we measure the thickness of Sheet$_2$ using the zero-crossings method. The measured thickness is defined as the distance between the left and right sides of image edges, which are the zero-crossings of second directional derivatives combined with Gaussian blurring along the normal orientation of the sheet structure. In actual situations, Gaussian blurring is employed to reduce the effect of noise. In this study, we employ a 2D Hessian matrix-based filter to enhance the boundaries of the sheet structure $I_{\mathrm{model}}(X; \tau_1, \tau_0, \tau_2)$. Assume that $\nabla^2 I_{\mathrm{model}}(X; \tau_1, \tau_0, \tau_2, \sigma)$ is a Hessian matrix of $I_{\mathrm{model}}(X; \tau_1, \tau_0, \tau_2, \sigma)$ blurred by isotropic Gaussian function with a standard deviation σ, which can be written as:

$$\nabla^2 I_{\mathrm{model}}(X; \tau_1, \tau_0, \tau_2, \sigma) = \begin{bmatrix} \frac{\partial^2}{\partial x^2} I_{\mathrm{model}}(X; \tau_1, \tau_0, \tau_2, \sigma) & \frac{\partial^2}{\partial x \partial y} I_{\mathrm{model}}(X; \tau_1, \tau_0, \tau_2, \sigma) \\ \frac{\partial^2}{\partial y \partial x} I_{\mathrm{model}}(X; \tau_1, \tau_0, \tau_2, \sigma) & \frac{\partial^2}{\partial y^2} I_{\mathrm{model}}(X; \tau_1, \tau_0, \tau_2, \sigma) \end{bmatrix}. \tag{11}$$

The second directional derivative along the normal direction of the sheet structure with respect to the image $I_{\mathrm{model}}(X; \tau_1, \tau_0, \tau_2, \sigma)$, is given by

$$I''_{\mathrm{model}}(X; \tau_1, \tau_0, \tau_2, \sigma, \vec{r}_\theta) = \vec{r}_\theta^{\,T} \nabla^2 I_{\mathrm{model}}(X; \tau_1, \tau_0, \tau_2, \sigma) \vec{r}_\theta. \tag{12}$$

Similarly, the directional first derivative along the normal direction of the sheet is given by

$$I'_{\mathrm{model}}(X; \tau_1, \tau_0, \tau_2, \sigma, \vec{r}_\theta) = \vec{r}_\theta^{\,T} \nabla I_{\mathrm{model}}(X; \tau_1, \tau_0, \tau_2, \sigma), \tag{13}$$

in which $\nabla I_{\mathrm{model}}(X; \tau_1, \tau_0, \tau_2, \sigma)$ is the gradient vector given by

$$\nabla I_{\mathrm{model}}(X; \tau_1, \tau_0, \tau_2, \sigma) = (I'_{\mathrm{model}_x}(X; \tau_1, \tau_0, \tau_2, \sigma), I'_{\mathrm{model}_y}(X; \tau_1, \tau_0, \tau_2, \sigma)). \tag{14}$$

Thickness measurement of the sheet structure can be performed only through analyzing the 1D profile of the second directional derivative $I''_{\mathrm{model}}(X; \tau_1, \tau_0, \tau_2, \sigma, \vec{r}_\theta)$ along the straight line. By substituting Eq. (9) for X in $I''_{\mathrm{model}}(X; \tau_1, \tau_0, \tau_2, \sigma, \vec{r}_\theta)$, the second directional derivative along the line can be written as:

$$I''_{\mathrm{model}}(s; \tau_1, \tau_0, \tau_2, \sigma) = I''_{\mathrm{model}}(s \cdot \vec{r}_\theta; \tau_1, \tau_0, \tau_2, \sigma, \vec{r}_\theta). \tag{15}$$

Similarly, the first derivative along the line can be written as:

$$I'_{\mathrm{model}}(s; \tau_1, \tau_0, \tau_2, \sigma) = I'_{\mathrm{model}}(s \cdot \vec{r}_\theta; \tau_1, \tau_0, \tau_2, \sigma, \vec{r}_\theta). \tag{16}$$

Fig. 3a shows the 1D profiles of the second derivative responses and thickness determination procedure using a zero-crossings method for the two adjacent sheet structures. We get zero-crossing points $s = q$ and $s = p$ on the left and right sides of the edges for Sheet$_2$, by solving $I''_{\mathrm{model}}(s; \tau_1, \tau_0, \tau_2, \sigma) = 0$ (shown in Fig. 3a). Let Zero-crossing

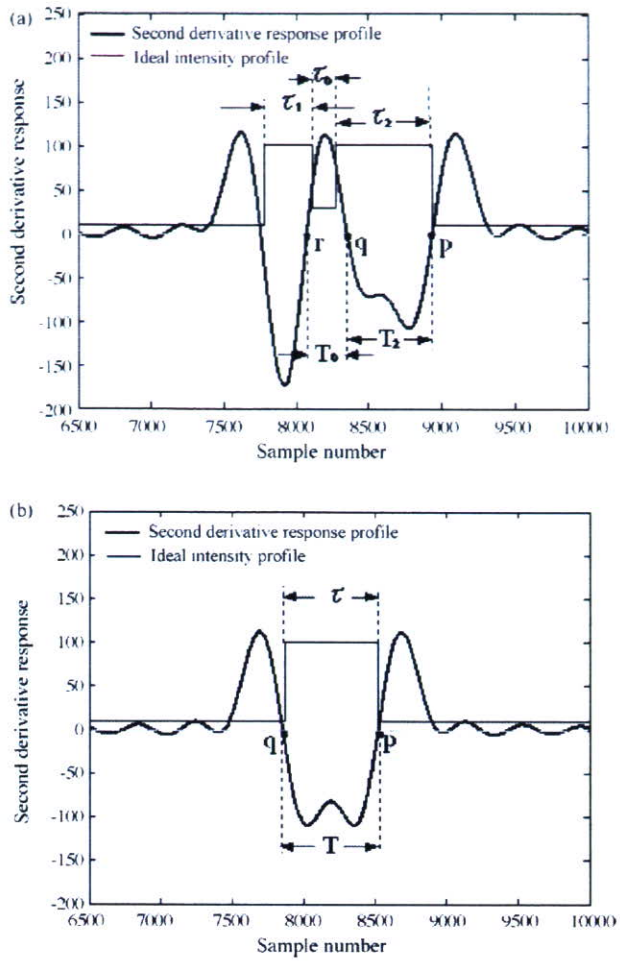

Fig. 3. Measured thickness of the sheet structures using zero-crossings method. The in-plane resolution: $\Delta_x = \Delta_y = 0.625$; Gaussian standard deviation: $\sigma = (1/2)\Delta_{xy}$ ($\Delta_{xy} = 0.625$ mm). $\tau_1 = 1.5$ mm, $\tau_0 = 0.5$ mm, $\tau_2 = \tau = 2.0$ mm. (a) Two adjacent sheets. Measured thickness of Sheet$_2$: $T_2 = |p - q|$. In the case of $\tau_0 = 0.5$ mm, thickness of $\tau_2 = 2.0$ mm was measured by approximately 1.76 mm (−12% error). Thickness of Sheet$_2$ was underestimated. (b) Single sheet. Measured thickness: $T = |p - q|$. Thickness of $\tau = 2.0$ mm was measured by approximately 2.05 mm (2.5% error).

points q and p correspond to the minimum and maximum values of $I'_{\text{model}}(s; \tau_1, \tau_0, \tau_2, \sigma)$ among those satisfying the condition given by $I''_{\text{model}}(s; \tau_1, \tau_0, \tau_2, \sigma) = 0$. The measured thickness, T_2, of Sheet$_2$ is defined as the distance between p and q, as follows:

$$T_2 = |p - q|. \tag{17}$$

In Fig. 3a, with $\tau_1 = 1.5$ mm, $\tau_0 = 0.5$ mm and $\tau_2 = 2.0$ mm, the true thickness $\tau_1 = 2.0$ mm is measured to be approximately 1.76 mm (−12% error). Fig. 3b shows the measured thickness of a single sheet. In Fig. 3b, the true thickness $\tau = 2.0$ mm is measured to be approximately 2.05 mm (2.5% error). Comparing Fig. 3a with Fig. 3b, it can be seen that measured thickness of Sheet$_2$ is underestimated as comparison with that of a single sheet.

2.2. Sample preparation and imaging

In the first experiment we imaged the four acrylic plate phantoms of sheet-like objects with known thickness. One was for a single sheet, the other three were used for two adjacent sheets with three different intervals of $\tau_0 = 0.5$, 1.0 and 1.5 mm, respectively.

(1) Single acrylic plate: Composed of four acrylic plates of 80 mm × 80 mm with true thickness $\tau = 2.0$, 1.0, 1.5, and 3.0 mm, placed parallel to each other with an interval of 30 mm (Fig. 4a).
(2) Two adjacent acrylic plates: each of the three phantoms consists of four pairs of acrylic plates, placed parallel with each other. Two adjacent acrylic plates thicknesses and the interval between them are given as follows:
   - Two adjacent sheets with τ_0 (interval between Sheet$_1$ and Sheet$_2$) = 1 mm: τ_2 (Sheet$_2$ thickness) = 2 mm, $\tau_0 = 1$ mm and τ_1 (Sheet$_1$ thickness) = 1.5 mm; $\tau_2 = 1$ mm, $\tau_0 = 1$ mm and $\tau_1 = 1.5$ mm; $\tau_2 = 1.5$ mm, $\tau_0 = 1$ mm and $\tau_1 = 1.5$ mm; $\tau_1 = 1.5$ mm, $\tau_0 = 1$ mm and $\tau_2 = 3$ mm (see from the top in Fig. 4b).
   - Two adjacent sheets with $\tau_0 = 0.5$ mm: $\tau_2 = 2$ mm, $\tau_0 = 0.5$ mm and $\tau_1 = 1.5$ mm; $\tau_2 = 1$ mm, $\tau_0 = 0.5$ mm and $\tau_1 = 1.5$ mm; $\tau_2 = 1.5$ mm, $\tau_0 = 0.5$ mm and $\tau_1 = 1.5$ mm; $\tau_1 = 1.5$ mm, $\tau_0 = 0.5$ mm and $\tau_2 = 3$ mm (not shown).
   - Two adjacent sheets with $\tau_0 = 1.5$ mm: $\tau_2 = 2$ mm, $\tau_0 = 1.5$ mm and $\tau_1 = 1.5$ mm; $\tau_2 = 1.0$ mm, $\tau_0 = 1.5$ mm and $\tau_1 = 1.5$ mm; $\tau_2 = 1.5$ mm, $\tau_0 = 1.5$ mm and $\tau_1 = 1.5$ mm; $\tau_1 = 1.5$ mm, $\tau_0 = 0.5$ mm and $\tau_2 = 3$ mm (not shown).

In the second experiment we imaged the two normal fresh-frozen cadaver hip joints (Fig. 5). After making bony defects artificially in the pelvis and the femur for landmarks, MR imaging was conducted in coronal direction with reference to the landmarks. After MR imaging, in order to obtain the anatomical thickness (See [6,14] for the detailed procedure of anatomical measurement), the hip joint was sectioned into halves, assuming an exact correlation to the imaging plane from the position of the landmarks.

MR imaging was performed with fat-suppressed 3D fast spoiled gradient-echo (SPGR) sequence on a 1.5 T MR system (Horizon, General Electric). A unilateral surface coil (TORSO, General Electric, Milwaukee, WI) was used. Four phantoms were scanned at two different in-plane rotation angles of $\theta = 0°$ and 30°. Each phantom was imaged in the sagittal plane; repetition time (TR)/echo time (TE) = 12.8/5.6 ms; flip angle = 5°; filed of view (FOV) = 160 mm × 160 mm; matrix = 256 × 256; section thickness = 1.5 mm; number of signals acquired = 2; acquisition time = 6 min 34 s. Two cadaveric hips were imaged in the coronal plane; TR/TE = 24.4/5.7 ms; flip angle = 20°; FOV = 160 mm × 160 mm; matrix = 256 × 256; section thickness = 1.5 mm; number of signals acquired = 2; acquisition time = 10 min 17 s.

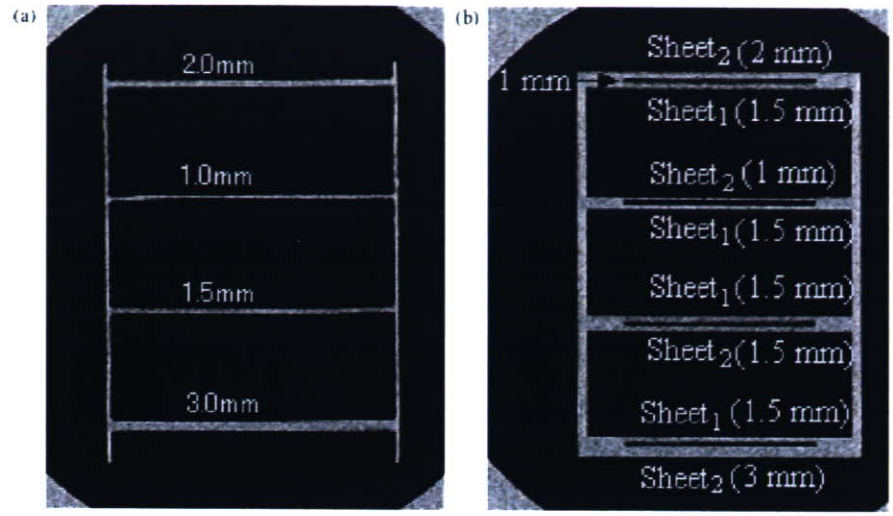

Fig. 4. MR images of acrylic plate phantoms. The horizontal and vertical axes of the images correspond to the y- and x-axis, respectively. (a) Single acrylic plate at an in-plane rotation angle of $\theta = 0°$. Thickness of Sheet$_1$ is 1.5 mm (not shown), and thickness of Sheet$_2$ is shown.

2.3. Actual thickness determination by zero-crossings method

Zero-crossings method was evaluated by using phantoms and cadaveric human hip joints. The postprocessing procedures for thickness measurement are given below. See Fig. 6 for a complete overview of thickness measurement.

2.3.1. Interpolation

In order to improve the in-plane resolution, we apply interpolation along the x- and y-directions. There are various alternative interpolation methods, but only sinc interpolation [15,16] guarantees the recovery of original information. In this experiment, sinc interpolation is used along the x- and y-directions to make the image matrix size double in the frequency domain. The sampling interval in the interpolated data is 0.3125 ($= \Delta = (1/2)\Delta_{xy}$) mm in the x-, and y-directions.

2.3.2. Extraction of sheet structure

In the actual images, it is necessary to extract the initial sheet regions before thickness determination. Using an automated segmentation technique [17,18], the approximated segmented regions of the sheets are extracted.

2.3.3. Thickness determination

For the extracted sheet structure, the boundaries of sheet structure surface are enhanced using Hessian matrix filter. This image filtering is based on the generally acknowledged theory that an edge corresponded to an abrupt change in image function, and that the first derivative should have an extreme and the

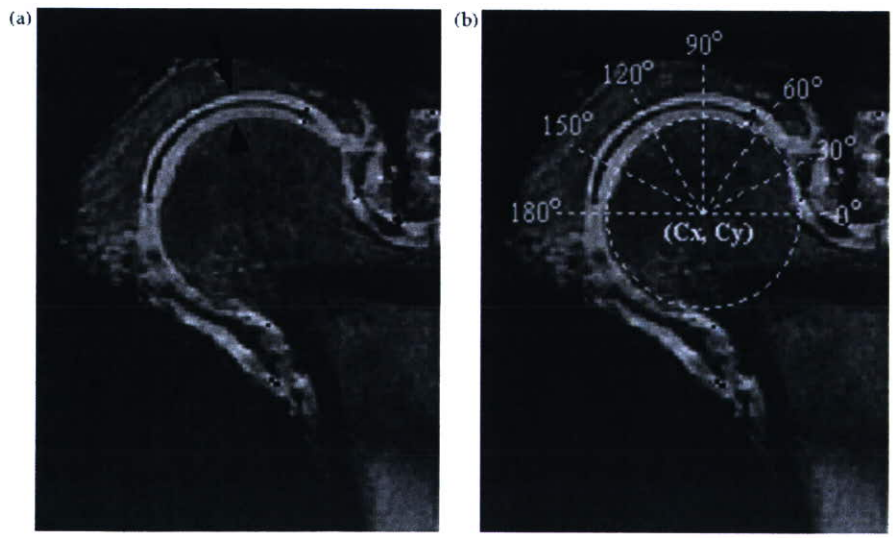

Fig. 5. Coronal MR images of a cadaver hip joint. (a) Original image. The femoral cartilage (arrowhead) is close to the acetabular cartilage (arrow). (b) Circle fitting method was employed to find the center (C_x, C_y) of the femoral head, and solid lines were drawn from this center.

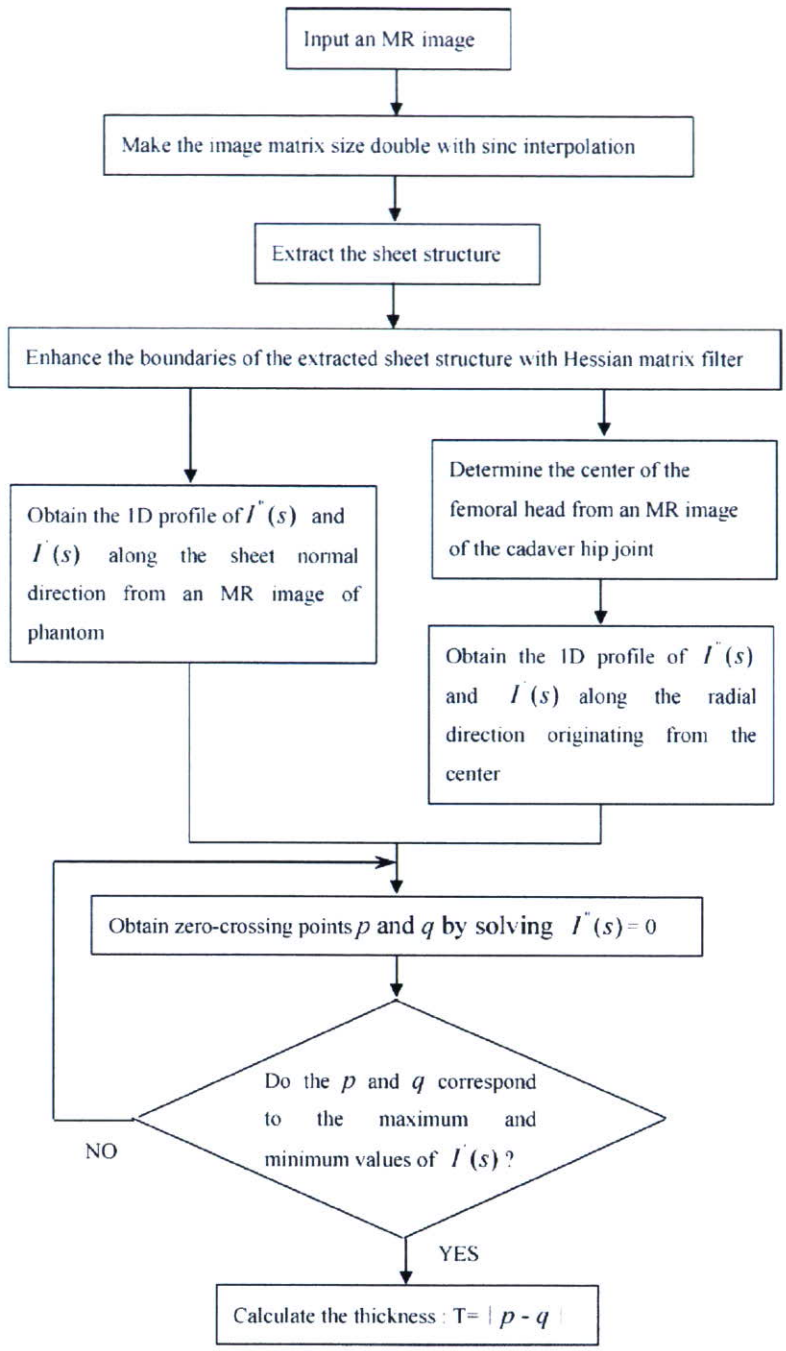

Fig. 6. Flow chart illustrating step for measuring the thickness of sheet structure using zero-crossings method.

second derivate should be equal to zero at the position of the edge.

In the experiments using the acrylic plate phantoms, the 1D profiles of the first directional derivative $I'(s)$ and the second directional derivative $I''(s)$ are obtained along the normal direction of sheet structure (acrylic plate). In the experiments using the hip joints (Fig. 5a), a circle fitting method is employed to find the center (C_x, C_y) using the boundaries of the femoral head (Fig. 5b). The 1D profiles of $I'(s)$ and $I''(s)$ are obtained along the radial direction originating from the center. Similar to Section 2.1.4, we get zero-crossing points $s = q$ and $s = p$ on the left and right sides of the edges for the sheet structure by solving $I''(s) = 0$. Let Zero-crossing points q and p correspond to the minimum and maximum values of $I'(s)$ among those satisfying the condition given by $I''(s) = 0$. The measured thickness of sheet structure is defined as the distance between p and q.

2.4. Improvement of measurement accuracy

As described in Section 2.1.4, zero-crossings method can yield large measurement errors for two adjacent sheet structures. To correct the measurement errors, we propose a new measure-

ment method based on a model of the scanning process. We model the scanning process for the two adjacent sheets and use this model to predict the shape of gray-level profiles along the sheet normal direction given in Eq. (10). The difference between the predicted profile and the actual profile observed in the MR data is minimized by refining the model parameters. The set of parameters that minimizes the difference between the model and the actual data yields the thickness estimation of the sheet structure.

We assume that D_t, D_0 and D_b are constant, while τ_1, τ_0 and τ_2 are variable at the different locations in the hip joint. We use zero-crossings method for estimating τ_1, τ_0 and τ_2. Because D_t, D_0 and D_b are constant in the entire image, if we have found one location where measured values of τ_1, τ_0, and τ_2 are regarded as a good approximation of true values τ_1, τ_0 and τ_2, D_t, D_0 and D_b at this location can be estimated accurately using this accurately measured values of τ_1, τ_0, and τ_2. In our case, when measured values of τ_1, τ_0 and τ_2 are 1.35 mm or above, these measured values can be regarded as a good approximation of their true values (this will be confirmed later in Section 3.1). If we might find several locations that satisfied the condition mentioned above, all D_t, D_0 and D_b estimated at these locations are averaged, respectively, and these average values are regarded as the estimated values of D_t, D_0 and D_b. Furthermore, τ_1, τ_0 and τ_2 at all locations are estimated accurately using D_t, D_0 and D_b obtained above, since D_t, D_0 and D_b are constant in the entire image. Briefly, the estimation procedure involves the following two steps: (1) the density values of D_t, D_0 and D_b are estimated with the accurately measured values of τ_1, τ_0 and τ_2; and 2) τ_1, τ_0 and τ_2 are estimated using D_t, D_0 and D_b estimated in the first step. See Fig. 7 for a complete overview for measuring the thickness using the improved method.

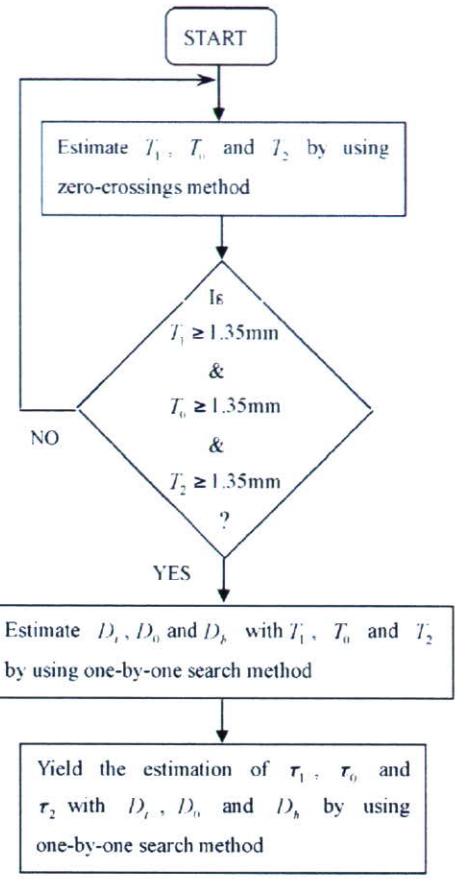

Fig. 7. Flow chart illustrating step for measuring the thickness of sheet structure using the improved method (one-by-one search method).

2.4.1. Estimation of D_t, D_0 and D_b

To estimate the density values of D_t, D_0 and D_b, the gray-level profile observed in the actual data needs to be fit to the modeled profile. Using the model of the MR imaging process, we can obtain the 1D profile of the predicted gray-level $I_{\text{model}}(s; \tau_1, \tau_0, \tau_2)$ (given in Eq. (10)) from $I_{\text{model}}(X; \tau_1, \tau_0, \tau_2)$ along the sheet normal direction $\vec{r}_\theta$. Similarly, 1D profile of the actual gray-level $I(s)$ is derived from MR image $I(X)$ along $\vec{r}_\theta$. The reconstruction of 1D profile $I(s)$ is performed at the subpixel resolution by using a bilinear interpolation.

Let T_1, T_0 and T_2 denote measured values of true values τ_1, τ_0 and τ_2, respectively, as estimated by zero-crossings method. In our case, for $T_1 \geq 1.35$ mm, $T_0 \geq 1.35$ mm and $T_2 \geq 1.35$ mm, these measured values are regarded as a good approximation of τ_1, τ_0 and τ_2. Let the observed profile be sampled at N discrete points in the actual image. With T_1, T_0 and T_2 satisfied the condition $T_1 \geq 1.35$ mm, $T_0 \geq 1.35$ mm and $T_2 \geq 1.35$ mm, D_t, D_0 and D_b are estimated by finding the values of D_t, D_0 and D_b minimizing

$$E(D_t, D_0, D_b) = \sum_{i=1}^{N} \{I(s_i) - I_{\text{model}}(s_i; T_1, T_0, T_2, D_t, D_0, D_b)\}^2. \quad (18)$$

where s_i is the ith sample along the sheet normal direction in the actual image. An optimization technique based on the Levenberg-Marquardt algorithm is used to solve this non-linear least square problem. Initial estimations of model parameters are required to start the optimization process. The initial values for D_t, D_0 and D_b are determined from the gray-level of MR image. We assume that D_t, D_0 and D_b are not locally variable and thus those are obtained as averages of all the results from the sequences of the gray-level profiles.

2.4.2. Estimation of τ_1, τ_0 and τ_2

Using estimated D_t, D_0 and D_b in the first step, τ_1, τ_0 and τ_2 are searched minimizing

$$E(\tau_1, \tau_0, \tau_2) = \sum_{i=1}^{N} \{I(s_i) - I_{\text{model}}(s_i; \tau_1, \tau_0, \tau_2, D_t, D_0, D_b)\}^2. \quad (19)$$

One drawback for Levenberg-Marquardt algorithm is the fact that the initial values of the model parameters are required to start the optimization process, and using the poor initial values can give rise to large estimation biases. As shown in Fig. 3a, the zero-crossings method exhibited considerable estimation biases for the two adjacent structures. To this end, the one-by-one search (exhaustive combination search) method is used for minimize

Eq. (19). In this study, τ_1 and τ_2 are discretized from 0.5Δ to 30Δ with 0.02Δ fixed interval ($\Delta = 0.3125$ mm), respectively, and τ_0 is discretized from 0.2Δ to 10Δ with 0.02Δ fixed interval. For all the combinations of discretized model parameters τ_1, τ_0 and τ_2, using the estimated D_t, D_0 and D_b in the first step, the cost function $E(\tau_1, \tau_0, \tau_2)$ given in Eq. (19) is calculated. Among all the combinations of the model parameters τ_1, τ_0 and τ_2, one combination of discretized model parameters τ_1, τ_0 and τ_2 corresponding to minimum value of cost function $E(\tau_1, \tau_0, \tau_2)$ is regarded as the estimations of τ_1, τ_0 and τ_2.

3. Experimental results

3.1. Measurement accuracy of zero-crossings method

3.1.1. Simulation and phantom measurements

Theoretical simulations confirm and explain that Sheet_1 affects the accuracy in the measured thickness of Sheet_2. To validate the theoretical simulations, we compare the simulated thickness with the average of actually measured thickness determined from MR images of acrylic phantoms. We also compare the measured thickness of Sheet_2 with that of a single sheet, assuming that the true thickness τ of a single sheet is the same as the true thickness τ_2 of Sheet_2. In the simulations, we mainly used the following parameters if not specified:

- True thickness of the sheet structures
  - * Two adjacent sheets: τ_1 (Sheet_1) = 1.5 mm, τ_2 (Sheet_2) = 0.5–3.0 mm.
  - * Single sheet: $\tau = \tau_2 = 0.5$–3.0 mm.
- Interval between two adjacent sheets: $\tau_0 = 0.25$–2.0 mm.
- Density values
  - * Two adjacent sheets: $D_t = 100$, $D_0 = 10$, $D_b = 0$.*Single sheet: D_5 (density value of sheet object) = 100, D_+ (density value of left-side background) = D_- (density value of right-side background) = 0.
- MR images resolution (square pixel): $\Delta_x = \Delta_y (= \Delta_{xy}) = 0.625$ mm.
- Guassian standard deviation: $\sigma = (1/2)\Delta_{xy}$.

Fig. 8 shows the results of simulation and phantom measurements. When the measured thickness values of a single sheet structure were 1.3 mm or above, these measured values could be regarded as a good approximation of their true thickness. Compared with the measured thickness of a single sheet structure, thickness of sheet structure influenced by adjacent sheet structure was considerably underestimated (Fig. 8a). The degree of underestimation of thickness was determined with the distance between the two adjacent sheet structures being less than 1.3 mm. The error between the simulated thickness and the average of actually measured thickness with phantoms of two adjacent sheets was smaller than 0.1 mm, and S.D. of actually measured thickness was within 0.1 mm (Fig. 8b). We also compared simulated thickness with the average of actually measured thickness with phantom of a single sheet. A good agreement between the simulation and phantom measurements was also observed (not shown). The numerical simulation

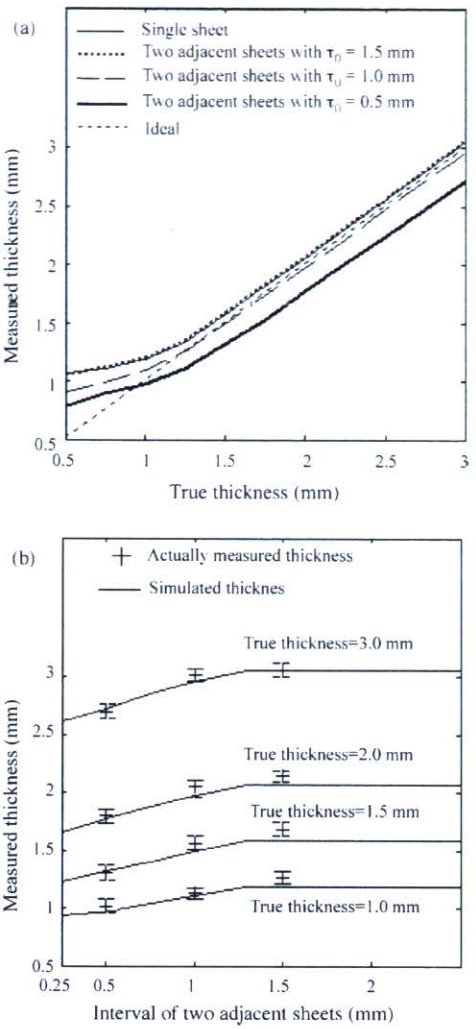

Fig. 8. Numerical simulation and phantom measurements with zero-crossings method. Gaussian standard deviation $\sigma = (1/2)\Delta_{xy}$ ($\Delta_{xy} = 0.625$ mm) and MR images of phantoms at $\theta = 0°$ were used. (a) Relationship between the measured thickness and the true thickness with simulation measurements. (b) Relationship between the measured thickness and the true interval of the two sheets. The measured thickness T_2 (average ± S.D.; $n = 50$) of phantoms also was shown. The error between the simulated thickness and the average of the actually measured thickness with phantoms was lower than 0.1 mm, and S.D. of the actually measured thickness was within 0.1 mm. The simulation was validated by phantom measurement.

was validated by experiments using actual MR images of phantoms.

Fig. 9 shows the relationship between the true interval τ_0 and the measured interval T_0 with a zero-crossings method. In Fig. 9, in the case of $\tau_1 = 1.5$ mm and $\tau_2 = 1.0$ mm, the interval between two sheets was measured. A good agreement between the simulated and the actually measured intervals was shown in Fig. 9. The results of Fig. 9 show that for measured interval value $T_0 \geq 1.3$ mm, these measured values were approximately equivalent to the true interval τ_0. Similarly, using $\tau_1 = 1.5$ mm and $\tau_2 = 1.5$, 2.0, and 3.0 mm, comparisons between τ_0 and T_0 were performed. The same results as Fig. 9 were observed.

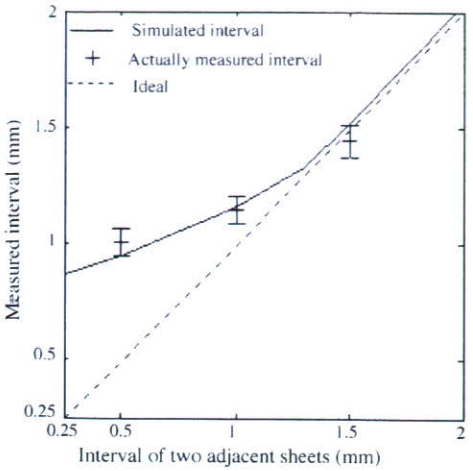

Fig. 9. Relation between the true interval τ_0 and the measured interval T_0 (average ± S.D.; $n = 50$) using a zero-crossings method. Guassian standard deviation $\sigma = (1/2)\Delta_{xy}$ ($\Delta_{xy} = 0.625$ mm) and MR images of a phantom at $\theta = 0°$ were used. Graph shows that for $T_0 \geq 1.3$ mm, these measured values are a good approximation of their true interval.

3.1.2. Measurements of cartilage thickness and joint space width

To specify how cartilage thickness and joint space width can be accurately measured by using zero-crossings method, we selected 10 positions in the anatomical section and in MR images, ranging from 135° to 150° (Fig. 5b) and performed the comparison of anatomic measurement and zero-crossings measurement (Table 1). The values of the examined 10 positions averaged $\tau_2 = 1.35 \pm 0.04$ mm at the anatomical sections and $T_2 = 1.36 \pm 0.08$ mm in an MR image for femoral cartilage thickness, $\tau_1 = 2.63 \pm 0.09$ mm at the anatomical sections and $T_1 = 2.56 \pm 0.12$ mm in an MR image for acetabular cartilage thickness, and $\tau_0 = 1.32 \pm 0.03$ mm at the anatomical sections and $T_0 = 1.36 \pm 0.06$ mm in an MR image for joint space width, respectively. From the experimental results we concluded that for the measured values of 1.35 mm or above, these values could be regarded as a good approximation of their true values. This is consistent with the results predicted by the numerical simulation.

3.2. Improvement of measurement accuracy

3.2.1. Phantom measurement

Fig. 10 shows the average measurement error and standard error for the zero-crossings, the improved methods at $\theta = 0°$ (Fig. 10a) and 30° (Fig. 10b). As shown in Fig. 10a and b, in the case of $\tau_1 = 0.5$ mm, the measured thickness of Sheet_2 was influenced by Sheet_1 when using a zero-crossings method. The improved method (one-by-one search method) gave measurements with less estimation bias than zero-crossings.

3.2.2. Cartilage thickness measurement

Linear regression and correlation analyses are carried out to examine the relationships between measurements obtained with our improved method and anatomical measurements, and between measurements obtained with zero-crossings method and anatomical measurements. The slope and the intercept of regression line are analyzed to determine the degree to which the two methods produced identical results. Regression equations are compared with the equation of the line of identity using t-statistics for the slope and the intercept. Differences in method measurement accuracy are assessed using paired t-tests. $p < 0.05$ was considered as the significant level for all statistical tests.

Fig. 11 indicates the determination procedures of the improved method for measurement of femoral cartilage thickness. The thickness of femoral cartilage was measured as 2.10 mm anatomically, 1.77 mm by zero-crossings method and 2.03 mm by the improved method. For accuracy determination, anatomical measurement of femoral cartilage thickness was set as reference. The improved method exhibited smaller estimation bias than zero-crossings method.

As shown in Fig. 12a, comparison of femoral cartilage thickness estimated by the zero-crossings method with the anatomical thickness produced a regression relationship ($y = 0.91x - 0.15$) with both the slop and the intercept differing significantly from one and zero, respectively ($p < 0.01$). The improved method shows a regression relationship ($y = 1.02x - 0.03$)

Table 1
Comparison of anatomic measurement and zero-crossings measurement

Positions	Anatomic measurement (mm)			Zero-crossings measurement (mm)		
	Femoral cartilage thickness	Joint space width	Acetabular cartilage thickness	Femoral cartilage thickness	Joint space width	Acetabular cartilage thickness
1	1.38	1.30	2.63	1.29	1.43	2.57
2	1.32	1.27	2.81	1.38	1.35	2.81
3	1.30	1.32	2.75	1.17	1.45	2.77
4	1.36	1.31	2.56	1.41	1.33	2.45
5	1.29	1.31	2.54	1.39	1.39	2.48
6	1.36	1.32	2.59	1.33	1.36	2.52
7	1.31	1.36	2.62	1.41	1.35	2.53
8	1.36	1.38	2.57	1.45	1.34	2.50
9	1.37	1.35	2.65	1.42	1.30	2.51
10	1.42	1.29	2.58	1.38	1.26	2.49
Mean	1.35	1.32	2.63	1.36	1.36	2.56

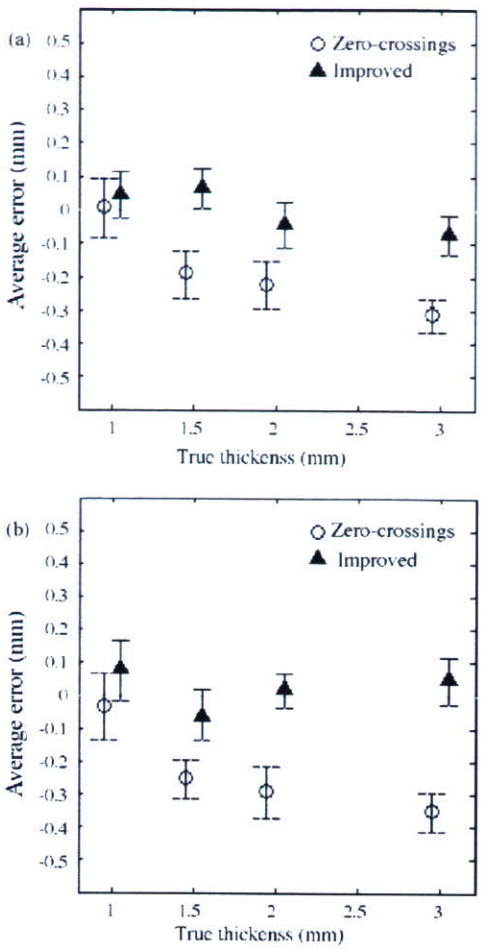

Fig. 10. Comparison of the average of measurement error (measured thickness-true thickness) obtained with the improved method to the average measurement error obtained with the zero-crossings method. Graph shows the average measurement error and standard error ($n = 50$). (a) In-plane rotation $\theta = 0°$. (b) In-plane rotation $\theta = 30°$.

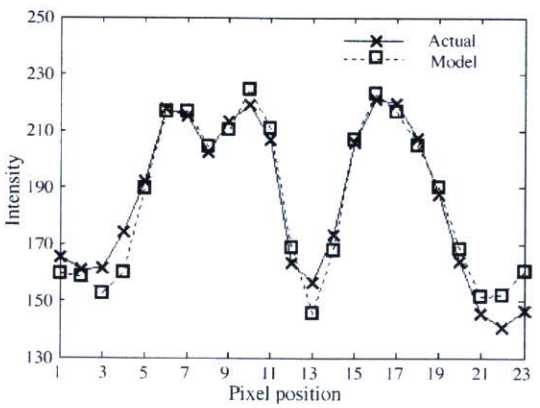

Fig. 11. Modeled gray-level profile and actual gray-level profile along the 100° radial direction (see Fig. 5b) after applying an optimization technique (one-by-one search algorithm). Femoral cartilage thickness, joint space width and acetabular cartilage thickness were estimated to be 2.10, 0.53 and 2.02 mm with the anatomical method, to be 1.77, 1.03 and 1.72 with the zero-crossings method, and to be 2.03, 0.41 and 2.15 mm with the improved method (one-by-one search algorithm).

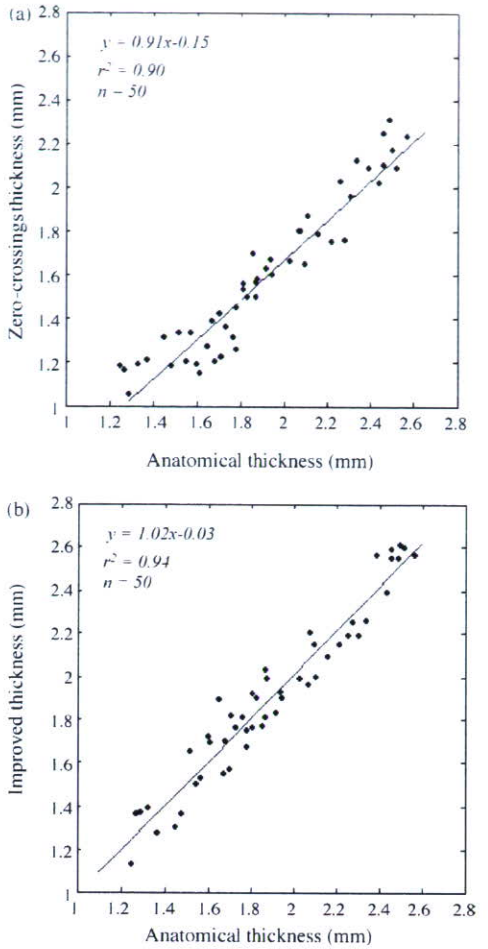

Fig. 12. Comparison of three methods for estimating the femoral cartilage thickness at the selected 50 positions with joint space width $\tau_0 < 1.25$ mm. (a) Cartilage thickness measured by zero-crossings method plotted against cartilage thickness measured by anatomic method at 50 positions. The line of best fit constructed at regression analysis and the corresponding regression equation also are shown. Linear regression analysis shows good agreement between cartilage thickness measured by zero-crossings method and that measured by anatomic method ($r_2 = 0.90$, $p < 0.01$). However, The slope (0.91) and intercept (-0.15) of the regression line was significantly different from one and zero, respectively ($p < 0.01$). The zero-crossings method underestimated the cartilage thickness in comparison to the anatomic measurement. (b) Cartilage thickness measured by the improved method plotted against cartilage thickness measured by anatomic method at 50 positions. The line of best fit constructed at regression analysis and the corresponding regression equation also are shown. Linear regression analysis yielded $r^2 = 0.94$, the slope and intercept of the regression line being 1.02 and -0.03, respectively. This shows that there is not only a strong linear relationship between the two measurements, but also very good agreement between the values obtained with both methods. A paired t-test shows the differences between the improved measurement from MR images and anatomic measurement is not statistically significant ($p > 0.1$).

closely approximating the line of identity with neither the slope nor the intercept (Fig. 12b). The anatomical measurement of cartilage thickness was used as the reference with which those obtained by the zero-crossings and improved measurements were compared. The results indicated that femoral cartilage thickness estimated using the improved method was significantly more accurate than that estimated by the zero-crossings method ($p < 0.01$). Fig. 13a shows the difference

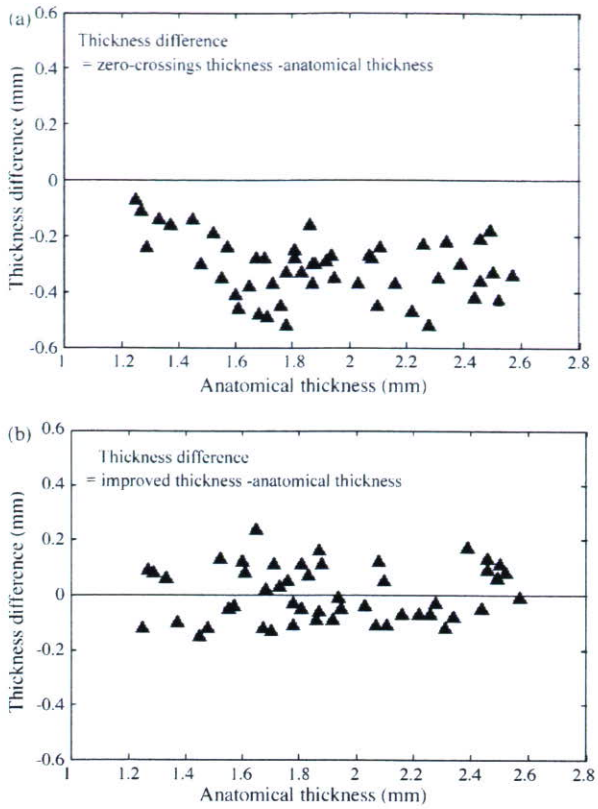

Fig. 13. Difference in the measured thickness between the methods. (a) Difference in the measured thickness between zero-crossings and anatomical methods. (b) Difference in the measured thickness between the improved and anatomical methods. The thickness of the femoral cartilage was estimated at 50 different positions along the radial direction originating from the center of the femoral head. Graph shows that the improved method gave the results similar to those presented from anatomical section, while the zero-crossings gave underestimation relative to the anatomical thickness.

in the measured thickness between the zero-crossings and anatomical methods. Fig. 13b shows the difference in the measured thickness between the improved and anatomical methods. Anatomical measurement of cartilage thickness was used as reference. The zero-crossings method gave considerable measurement bias (underestimating the cartilage thickness), while the improved method gave measurements with less estimation bias.

4. Discussion

As for two adjacent sheet structures ($Sheet_1$ and $Sheet_2$), such as femoral cartilage and acetabular cartilage in the hip joint, we performed the simulation measurement, phantom measurement and articular cartilage thickness measurement. The experimental results showed considerable underestimation in thickness measurement occurred due to the influence of the adjacent sheet structure. In order to remove the influence of the adjacent sheet and calibrate measurement bias, an improved measurement method was presented. The main findings of our work are as follows:

4.1. Observation of profiles by FWHM and zero-crossings methods

In order to clarify the cause of the influence of the adjacent sheet ($Sheet_1$) on the accuracy of thickness measurement of $Sheet_2$, we showed the profiles of thickness determination procedures using FWHM (see Fig. 2) and zero-crossings (see Fig. 3a) methods. The profiles of the two determination procedures distinctly exhibited the influence of the adjacent sheet on the accuracy of thickness measurement. Through observing the profiles produced by FWHM and zero-crossings methods, we can see that the adjacent sheet resulted in the underestimation of thickness. In this study, we further used zero-crossings method to analyze the measurement accuracy of the sheet structure thickness.

4.2. Effect of Gaussian standard deviation σ

In the actual image, Gaussian blurring is employed to remove the noise. The degree of smoothing is determined by the Gaussian standard deviation σ. Better effectiveness of Gaussian smoothing require larger the standard derivation of Gaussian. On the other hand, we should notice that larger standard derivation of Gaussian give rise to greater underestimation of thickness. In this study, we performed the thickness measurement with $\sigma = (1/2)\Delta_{xy}$, $\sigma = (\sqrt{2}/2)\Delta_{xy}$ (not shown) and $\sigma = \Delta_{xy}$ (not shown). When $\tau_0 > 3$–4σ, the accuracy of thickness measurement was not affected by the adjacent sheet. This means, the measured thickness of $Sheet_2$ was approximately the same as that of a single sheet.

4.3. The validity of the simulation

The results of phantom measurements and simulations showed that the bias between the actually measured thickness and the simulated thickness was nearly within 0.1 mm (see Fig. 8b). The validity of theoretical simulations was confirmed. Thus, we can use mathematical model of two adjacent sheets and MR imaging parameters to predict the measurement accuracy. Also, thickness measurement can be performed only through analyzing 1D profile of the second derivative responses along the normal direction of sheet surface, so the computation of the simulations is simplified and its cost is drastically reduced.

4.4. Normal direction of the cartilage surface

In the present study, two healthy cadaveric specimens of human hip were used for determining the femoral cartilage thickness. We assume that the shape of the femoral head approximates the exact sphere. Therefore, we employed a circle fitting method to find the center using the boundaries of the femoral cartilage. The radial directions from the detected center can be regarded as the normal direction of the cartilage surface. However, as in the case of diseased hip joint, because the shape of the femoral head is not perfectly spherical, this method cannot be used. In such cases, the normal direction

might be estimated using the eigenvectors of the Hessian matrix [19].

4.5. An improved measurement method

To improve the accuracy of thickness measurement, we developed a new technique based on a model of the MR imaging process for two adjacent sheet structures separated by a small distance. Thickness estimation problem is formulated as a least square fitting of an actual gray-level profile observed in the MR data set to a modeled gray-level profile. The difference between the modeled profile and the actual gray-level profile observed in the MR data is minimized by refining the model parameters. We employed an exhaustive one-by-one search algorithm to minimize this difference, not using the Levenberg-Marquardt algorithm. One drawback for Levenberg-Marquardt algorithm is the fact that the initial values of the model parameters are required to start the optimization process, and using the poor initial values can give rise to large estimation biases. The zero-crossings method exhibited considerable estimation biases for the two adjacent sheet structures (see Fig. 8). An attempt was made to obtain the initial values of τ_1, τ_0, and τ_2 using zero-crossings method. Levenberg-Marquardt algorithm yielded the poor estimations of τ_1, τ_0, and τ_2 when applying the zero-crossings method to obtain the initial values. Thus, one-by-one search method was used to minimize the difference between the modeled profile and the actual gray-level profile observed in the MR data.

Our new improved technique is not only available for two adjacent sheets but also available for a single sheet. There are inherent limitations on the accuracy in thickness measurement of a single sheet due to finite spatial resolution of imaging scanners and blurring involved in edge detections [20,21]. For two adjacent sheets, there is a limitation of the influence of the adjacent sheet, as well as those mentioned above. Our improved method can overcome these limitations. Using zero-crossings method, for the sheet structure affected by the adjacent sheet, the measured thickness value is an underestimation relative to its true thickness, whereas for the unaffected sheet with a small thickness, its measured value is an overestimation relative to its true thickness (see Fig. 8). The improved method gave the accurate measurements in both cases.

In conclusion, in this paper, we confirmed that for two adjacent sheet structures, considerable underestimation in thickness measurement occurred due to the influence of the adjacent sheet structure. A new technique based on a model of the MR imaging process was proposed to improve the measurement accuracy. In our present work, in the case of isotropic resolution, measurement accuracy analysis and improvement of accuracy were performed. In generally, the resolution of medical 3D data along z-direction (the direction perpendicular to the slice plane) is lower than within slices, this means that the voxel of 3D image is anisotropic. Therefore, in the future work, the effect of anisotropic voxel on measurement accuracy requires investigation, and then the calibration of measurement bias would be needed to perform. Finally, our work will focus on clinical validation using a large set of data for applications.

5. Summary

In the hip joint, in which the femoral and acetabular cartilages are adjacent to each other. To investigate whether the accuracy in thickness measurement of femoral cartilage is influenced by acetabular cartilage, we developed a mathematical model for two adjacent sheet structures, which simulated the femoral and acetabular cartilages in the hip joint. MR imaging process and post\processing for thickness measurement are also modeled and simulated. Thickness is defined as the distance between the two sides of the edges, which are the zero-crossing points of the second derivatives combined with Gaussian blurring along the normal direction. The result of simulation measurements shows that considerable underestimation in thickness measurement occurred due to the influence of the adjacent sheet structure. In order to remove the influence of the adjacent sheet and calibrate measurement bias, we propose a new measurement method based on a model of the MR imaging process. Using this model, we can predict the shape of the gray-level profile along the normal direction of the sheet surface. Thickness estimation problem is formulated as a least square fitting of an actual gray-level profile observed in the MR data set to a predicted gray-level profile. Using a one-by-one search (exhaustive combination search) technique, the model parameters are adjusted to minimize the differences between the predicted and the actual gray-level profiles observed in the MR data. The set of parameters that minimizes the differences yields the thickness estimation of the sheet structure. In the experiments, we imaged the acrylic plate phantoms and two normal cadaver hip joints. All MR images were acquired with a resolution of 0.625 mm × 0.625 mm × 1.5 mm. In the first experiment, we tested the accuracy of the conventional zero-crossings method using phantoms. The result of phantom measurements shows that the zero-crossings method underestimated the thickness of two adjacent sheet structures. The error between simulation measurement and phantom measurement was smaller than 0.1 mm, and S.D. of actually measured thickness was within 0.1 mm. A good agreement between the simulation and phantom measurements was observed. The numerical simulation was validated by experiments using actual MR images of phantoms. In the second experiment, we performed the comparison of the zero-crossings method and the new improved method. In the experiment using phantoms, the results show that our new improved method was more accurate than zero-crossings method. In the experiment using two cadaveric human hip joints, the results obtained by the new improved method for cartilage thickness measurement were significantly different from those generated by zero-crossings method ($p < 0.01$) and were more accurate when compared using paired t-tests. In conclusion, in this paper, we confirmed that for two adjacent sheet structures, considerable underestimation in thickness measurement occurred due to the influence of the adjacent sheet structure. Using phantoms and two normal cadaver hip joints, we present results showing that the new improved method removed the influence of the adjacent sheet and was more accurate than the conventional zero-crossings method in estimating thickness of two adjacent sheet structures.

Acknowledgements

This work was partly supported by the Japan Society for the Promotion of Science (JSPS Research for the Future Program and JSPS Grant-in-Aid for Scientific Research (c) (2) 11680389). We are grateful to Doctor Hisashi Tanaka, Department of Radiology, Osaka University Graduate of Medicine, Japan, who provided the MR image Data.

References

[1] McWalter EJ, Wirth W, Siebert M, et al. Use of novel interactive input devices for segmentation of articular cartilage from magnetic resonance images. OsteoArthritis Cartilage 2005;13:48–53.
[2] Koo S, Gold GE, Andriacchi TP. Considerations in measuring cartilage thickness using MRI: factors influencing reproducibility and accuracy. OsteoArthritis Cartilage 2005;13:782–9.
[3] Sabine W, Thomas M, Wilhelm H, et al. Quantitative assessment of patellar cartilage volume and thickness at 3. 0 Tesla comparing a 3D-fast low angle shot versus a 3D-true fast imaging with steady-state precession sequence for reproducibility. Invest Radiol 2006;41:189–97.
[4] Eskstein F, Charles HC, J.Buck R, et al. Accuracy and precision of quantitative assessment of cartilage morphology by Magnetic Resonance Imaging at 3.0 T. Arthritis Rheum 2005;52:3132–6.
[5] Gougoutas AJ, Wheaton AJ, Borthakur A, et al. Cartilage volume quantification via live wire segmentation. Acad Radiol 2004;11:1389–95.
[6] Nishii T, Sugano N, Sato Y, et al. Three-dimensional distribution of acetabular cartilage thickness in patients with hip dysplasia: a fully automated computational analysis of MR imaging. Osteoarthritis Cartilage 2004;12:650–7.
[7] Takao M, Sugano N, Nishii T, et al. Application of three-dimensional magnetic resonance image registration for monitoring hip joint diseases. Magn Reson Imaging 2005;23:665–70.
[8] Nakanishi N, Tanaka H, Nishii T, et al. MR evaluation of the articular cartilage of the femoral head during traction. Acta Radiol 1999;40:60–3.
[9] Krissian K, Malandain G, Ayache N, et al. Model-based detection of tubular structures in 3-D images. Comput Vision Image Understanding 2000;80:130–71.
[10] Parker DL, Du YP, Davis WL. The voxel sensitivity function in Fourier transform imaging: applications to magnetic resonance angiography. Magn Reson Med 1995;33(2):156–62.
[11] Schwab RJ, Gefter WB, Kline LR, et al. Dynamic imaging of the upper airway during respiration in normal subjects. J Appl Physiol 1993;74:1504–14.
[12] Amirav I, Kramer SS, Grunstein MM, et al. Assessment of methacholine induced airway constriction by ultrafast high-resolution computed tomography. J Appl Physiol 1993;75:2239–50.
[13] Kramer SS, Hoffman EA, Amirav I. High resolution CT assessment of pediatric airways: structure and function. In: Proceedings of the SPIE Conference on Medical Imaging. Newport Beach, CA 1994;2168:13-8.
[14] McGibbon CA, Bencardino J, Yeh ED, et al. Accuracy of cartilage and subchondral bone spatial thickness distribution from MRI. J Magn Reson Imaging 2003;17:703–15.
[15] Hylton NM, Simovsky I, Li AJ, et al. Impact of section doubling on MR angiography. Radiology 1992;185(3):899–902.
[16] Du YP, Parker DL, Davis WL, et al. Reduction of partial-volume artifacts with zero-filled interpolation in three-dimensional MR angiography. J Magn Reson Imaging 1994;4(5):733–41.
[17] Sato Y, Westin CF, Bhalerao A, et al. Tissue classification based on 3-D local intensity structures for volume rendering. IEEE Trans Visual Comput Graph 2000;6:160–80.
[18] Sato Y, Kubota T, Nakanishi K, et al. Three-dimensional reconstruction and quantification of hip joint cartilages from magnetic resonance images. Lecture Notes in Computer Science, Berlin Germany, Proc MICCAI'99. LNCS 1999;1679:338–47.
[19] Sato Y, Tamura S. Detection and quantification of line and sheet structures in 3-D images. Lecture Notes in Computer Science, Berlin Germany, Proc MICCAI2000. LNCS 2002;1935:154–65.
[20] Dougherty G, Newman D. Measurement of thickness and density of thin structures by computed tomography: a simulation study. Med Phys 1999;26(7):1341–8.
[21] Prevrhal S, Fox JC, Shepherd JA, et al. Accuracy of CT-based thickness measurement of thin structures: modeling of limited spatial resolution in all three dimensions. Med Phys 2003;30:1–8.

Yuanzhi Cheng entranced into Graduate School of Mechatronics Engineering at Harbin Institute of Technology in 2002. He is currently completing the Ph.D. from Harbin Institute of Technology Graduate School of Mechatronics Engineering and Osaka University Graduate School of Medicine.

Shuguo Wang received the B.S., M.S., and the Ph.D. degrees in Mechatronics from the Harbin Institute of Technology, Harbin, China. He has assumed the position of Professor at the School of Mechatronics Engineering at the Harbin Institute of Technology since 1992. He has published more than 100 papers in scientific journals. Professor Wang served as the Chair/Co-Chair on the many National and International Robotics Conference and also served on the National Science Foundation's Robotics Council from 1998 to 2005. In 1995, he received the Outstanding Senior Faculty Research Award from the Ministry of Education of China.

Takaharu Yamazaki received the B.S. and M.S. degrees from the Department of Medical Physics and Engineering in Allied Health Science and Ph.D. degree in Medical Science from Osaka University, Japan in 1998, 2000 and 2004, respectively. From 2004 to 2006 he was a Research Associate at the Department of Orthopaedics at Osaka University Graduate School of Medicine. Since 2006, he has been a Specially Appointed Lecturer at the Center for Advanced Medical Engineering and Informatics, Osaka University. His research interests include medical image processing and analysis, kinematics of skeletal joint, and biomechanics.

Jie Zhao received the Ph.D. degree from the Harbin Institute of Technology, Harbin, China in 1997. He is currently a Professor in Mechatronic Engineering Department Robotics Institute, Harbin Institute of Technology. Dr. Zhao is a member of the Intelligent Robot Professional Committee of China Artificial Intelligence Association. His research interests are concentrated on the multi-sensor integrated and control system technology, robotic teleoperation technology, medical robot technology, and bionic robotics.

Yoshikazu Nakajima received B.S. and M.S. degrees from Fukui University in1992 and 1994, respectively, and a Ph.D. degree from Osaka University in 1997. He is currently an Associate Professor of the Department of Bioengineering, School of Engineering, the University of Tokyo. He is also with the Department of Engineering Synthesis at School of Engineering and the Intelligent Modeling Laboratory, the University of Tokyo. His research interests include medical image processing, computer-integrated surgical systems and surgical informatics.

Shinichi Tamura received the B.S., M.S., and Ph.D. degrees in Electrical Engineering from Osaka University, Osaka, Japan, in 1966, 1968, and 1971, respectively. He is currently a Professor at the Graduate School of Medicine, Graduate School of Information Science and Technology, and the Center for Advanced Medical Engineering and Informatics, Osaka University. He has published more than 250 papers in scientific journals and received several awards from journals including Pattern Recognition and Investigative Radiology. His current research activities include works in the field of medical image analysis and its applications. Currently he is an Editorial Board member of International Journal of Computer Assisted Radiology and Surgery. Dr. Tamura is a member of the Institute of Electronics, Information and Communication Engineers of Japan, the Information Processing Society of Japan, the Japanese Society of Medical Imaging Technology, and the Japan Radiological Society.

2-3-1

放射光を用いた暗視野法による関節軟骨の透視撮影法および断層撮影法の開発

浦定 俊之[1]　安藤 正海[2]　杉山 弘[2]　島雄 大介[1]
武田 健[1]　尾崎 敏文[1]

【目的】変形性関節症に代表される軟骨変性を正確に評価することは，現在の画像診断法では限界がある．関節軟骨の画像診断に関する研究はいくつか報告されているが，投影法による画像診断法の報告はほとんどない．われわれは，独自に開発したX線暗視野法を用いた関節軟骨のX線撮影を行い，過去に報告してきた．今回，新たに透視撮影法に成功したので報告する．

【方法】大型放射光施設SPring-8(BL20B2)，および高エネルギー加速器研究機構(PF, BL14B)で実験を行った．暗視野法とは，屈折コントラスト法を応用したX線画像である．被写体にX線を照射し，物体で屈折したX線を回折アナライザーによって分離し，屈折X線だけで画像化する方法である．通常のX線画像(吸収コントラスト)では写らない被写体を撮影することが可能である．解剖体遺体から摘出した皮膚，軟部組織が付着したままのPIP関節，肩関節，膝関節を用いて，表面入射型CCD(浜松ホトニクス社)を用いて，透視撮影，断層撮影を行った．

【結果と考察】今までの原子核板を用いた撮影で，指，肩，膝の各関節軟骨の鮮明な撮影が可能であった．原子核板による撮影は高い解像度であるが，現像に時間がかかるため，条件設定(X線照射角度や撮影条件など)にある程度の時間が必要であった．また，コストが高い点も問題となる．この欠点を改善するために，透視撮影法を開発した．このシステムを用いることで，条件設定がリアルタイムで可能となり，よりよい軟骨の画像がすばやく撮影可能となった．また，断層撮影法の開発も同時に行ってきており，この透視撮影法を用いることで，大幅に撮影時間を短縮することが可能となった．透視撮影により関節軟骨の画像がリアルタイムで得られるため，関節軟骨の動的解析にも有用なシステムであると考えている．さらに，断層撮影にも有用なシステムであり，軟骨変性の局在が画像診断可能と考えられる．現在，このシステムを利用することで，関節軟骨のCT撮影法に開発に取り組んでいる．

[1]岡山大学院整形　[2]東京理科大TDLS研究センター
[3]高エネルギー加速器研究機構　[4]茨城県立医療大放射線技術科学科

2-3-2

超音波を用いたTime of Flight法による関節軟骨の音速測定

大橋 暁[1]　大西 五三男[1]　酒井 亮一[2]　廣田 浩二[1]
宮坂 好一[1]　中村 耕三[1]

【背景・目的】超音波による関節軟骨定量診断法を確立するためには軟骨音速の高精度測定が必要である．予備的に豚膝関節軟骨を用いて音速測定を行い，開発した測定法の精度を検証した．

【方法】屠畜による音速差を考慮し，生後6カ月と3年の豚を用いた．屠畜後約3℃にて3日間冷蔵保存後，被検体を切断し−20℃にて冷凍保存した．室温において生食により解凍し，大腿骨顆部の骨軟骨片を採取した．これをPanametrics社製の超音波送受信機(NDT-5800)と10 MHzのシングルプローブ(NDT-M311)を用い，脱気水(21℃)内で9点においてRadiofrequency(RF)信号を観察した．信号はオシロスコープ(TDS 3054, Tektronix)を介してコンピューターに記録し，軟骨表面境界，軟骨深層-石灰化軟骨境界(tidemark)に相当する各反射波の包絡線ピークを求め，peak-to-peak法により超音波飛翔時間(TOF, time of flight)を計測した(測定精度：±0.2 ns)．ダイシングソーを用い骨芽検出点が断面となるような骨軟骨切片を作成(n=3)し，顕微鏡(MM-22, Nikon)により各点における軟骨表面からtidemarkまでの距離を軟骨厚として測定した(測定精度：±4 μm)．また，TOFおよび顕微鏡計測の軟骨厚をもちいて軟骨音速を算出した(測定精度：±3 m/s)．

【結果】TOFは子豚，成豚それぞれ3.455−0.178 μs(平均±SD)，1.355±0.060 μs，軟骨厚は2.567±0.084 mm，1.161±0.037 mmであった．軟骨音速はそれぞれ1488±9 m/s，1717±104 m/sであり，成豚の音速が有意に速かった($p<0.01$，t検定)．また，本測定法の変動係数(CV)は，子豚，成豚それぞれ3.2%，6.1%であった．

【考察】成豚の軟骨音速は先行研究の値に近い値であった．本測定法は精度が高く，実用性が高いと考える．

[1]東大大学院整形　[2]アロカ株式会社研究所

2-3-3

変形性膝関節症における診断システムの開発

[illegible]敬之[1]　村木 重之[1]
[illegible]口 浩[2]　中村 耕三[1]

【目的】変形性関節症は疾患であるが，その病重症度の評価方法も存法を駆使して，変形性膝数の重症度指標を自動断システムKOACAD(nosis)を確立し，OAスを用いて，その精度た．

【方法・結果】立位膝ルフィルタによるノ統計処理による基準・外側の関節裂隙の内側の骨棘面積(OP)に計測するソフトをトROADの計3，0た50膝についてその評価者間，評価者0.62-0.75であった．あった．続いて，Kトの60歳以上の痛群(1385膝)に分定で解析したとこそれぞれ内側mJS個JSA：<0.000FTA：<0.0001ィック回帰分析でと最も強い相関を-1.81)，女性1.4

【考察・結論】世界に先駆けては簡便に行える定のように，膝療の正確な評れる．

[1]東大22世紀医